Chinese Chemical Letters 37 (2026) 111656

Contents lists available at ScienceDirect

Chinese Chemical Letters

journal homepage: www.elsevier.com/locate/cclet

# Self-assembly of spin crossover Fe(II) framework materials with new topologies using tetra(pyridinyl)benzenediamine ligand

Guang Yang, Lu Yu, Ze-Yu Ruan, Ai-Qi Jian, Yan-Ru Chen, Yan-Cong Chen, Zhao-Ping Ni*, Ming-Liang Tong*

*Key Laboratory of Bioinorganic and Synthetic Chemistry of Ministry of Education, School of Chemistry, Institute of Green Chemistry and Molecular Engineering, Guangdong Basic Research Center of Excellence for Functional Molecular Engineering, Sun Yat-sen University, Guangzhou 510275, China*

ARTICLE INFO

*Article history:*
Received 25 April 2025
Revised 19 July 2025
Accepted 30 July 2025
Available online 5 August 2025

*Keywords:*
Spin crossover
Metal-organic framework
Cluster
Topology
Hysteresis

ABSTRACT

Spin crossover (SCO) metal-organic frameworks (MOFs) exhibit significant potential for applications in data storage, displays, switches, actuators and sensors. However, designing novel SCO MOFs with new framework topologies remains a considerable challenge. Herein, the self-assembly of $FeBr_2$ and $Fe(ClO_4)_2{\cdot}6H_2O$ with $K[Ag(CN)_2]$ and $N^1,N^1,N^3,N^3$-tetra(pyridin-4-yl)benzene-1,3-diamine (*i*-TPBA) resulted in two distinct MOFs: $[Fe^{II}{}_3\{Ag_8Br_8(CN)_6\}(i\text{-TPBA})_3]{\cdot}4DEF$ (**1**, DEF = *N*,*N*-diethylformamide) and $[Fe^{II}\{Ag(CN)_2\}(i\text{-TPBA})]ClO_4{\cdot}2H_2O{\cdot}0.5DEF$ (**2**). In **1**, the hexatopic cluster anions $[Ag_8Br_8(CN)_6]^{6-}$, tetratopic ligands *i*-TPBA and hexatopic Fe(II) ions are linked to form a cluster-based MOF with the **urk** topology. In contrast, the $[Ag(CN)_2]^-$ units in **2** axially bridge the Fe(II) ions, constructing one-dimensional right-handed $3_1$ helical chains, which are further linked by tetratopic *i*-TPBA connectors to generate a three-dimensional chiral framework with a previously unreported topology, designated as ***sco*1**. Moreover, the SCO behavior can be effectively modulated by thiophene guest molecules, leading to the observation of a rare scan rate-dependent hysteretic SCO behavior in **2_thio**. Thus, this study demonstrates that multidentate ligands can be employed to construct SCO MOFs with new topologies, offering a versatile platform for the advancement of multifunctional SCO materials

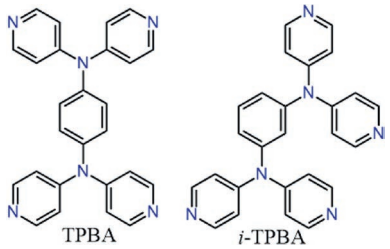
© 2026 Published by Elsevier B.V. on behalf of Chinese Chemical Society and Institute of Materia Medica, Chinese Academy of Medical Sciences.

Spin crossover (SCO) compounds are classic bistable materials that can reversibly switch between high-spin (HS) and low-spin (LS) states under external stimuli such as temperature, light and pressure. These materials hold significant potential for applications in data storage, displays, switches, actuators and sensors [1–4]. As a collective phenomenon, gradual, abrupt, hysteretic, step and incomplete SCO behaviors can be observed in the solid state. To achieve hysteretic SCO properties, strategies involving effective intermolecular interactions and covalent linker have been proposed [5,6]. Consequently, coordination polymers, including one-dimensional (1D) Fe(II)-triazole chains, two-dimensional (2D) $[Fe(NCX)_2(L)_2]$ families (X = S, Se or $BH_3$, L = bispyridyl ligands) and three-dimensional (3D) Hofmann-type metal-organic frameworks (MOFs) [4,7–10], have been extensively studied in the SCO field. Owing to their inherent porosity, MOFs are particularly noteworthy for their potential applications in gas storage, separation and catalysis [11–14], thereby enhancing the multifunctionality of SCO MOFs [15,16]. Most Hofmann-type MOFs have been confined to *fsc* and *pcu* topologies [17,18], limiting the expansion of their functional diversity. However, designing SCO MOFs with novel topologies remains a significant challenge.

Cluster-based MOFs are renowned for their diverse topologies and unique physicochemical properties [19–21]. Recently, we serendipitously synthesized the first example of cluster-based SCO MOFs [22], $[Fe_3\{Ag_8X_8(CN)_6\}(TPBA)_3]{\cdot}n$DMF (X = Br, $n = 9$ and X = I, $n = 8$, TPBA = *N*,*N*,*N*′,*N*′-tetra(pyridine-4-yl)benzene-1,4-diamine, Scheme 1), by reacting $FeX_2$ with TPBA and $K[Ag(CN)_2]$ in MeOH/DMF solution. The hexatopic cluster anions $[Ag_8X_8(CN)_6]^{6-}$, tetratopic ligands TPBA and hexatopic Fe(II) ions are interconnected to form the **urk** topology. Most intriguingly, the reaction of $Fe(ClO_4)_2{\cdot}6H_2O$ with TPBA and $K[Ag(CN)_2]$ in MeOH/DMF solution led to the formation of another cluster-based SCO MOF [23], $[Fe_3\{Ag_4(CN)_6(H_2O)\}_2(TPBA)_3](ClO_4)_2{\cdot}7DMF$. In this structure, the Fe(II) ions are axially bridged by the double interlocking $[Ag\{Ag(CN)_2\}_3(H_2O)]^{2-}$ clusters, forming inorganic connectivity with 2D → 3D *n*-fold Borromean entangled topology. Furthermore, the Fe(II) ions are equatorially linked by the tetratopic TPBA ligands, generating a 3D framework with the extremely rare **3,4,6-**

* Corresponding authors.
*E-mail addresses:* nizhp@mail.sysu.edu.cn (Z.-P. Ni), tongml@mail.sysu.edu.cn (M.-L. Tong).

https://doi.org/10.1016/j.cclet.2025.111656
1001-8417/© 2026 Published by Elsevier B.V. on behalf of Chinese Chemical Society and Institute of Materia Medica, Chinese Academy of Medical Sciences.




**Scheme 1.** Isomeric ligands used for the synthesis of cluster-based SCO MOF.

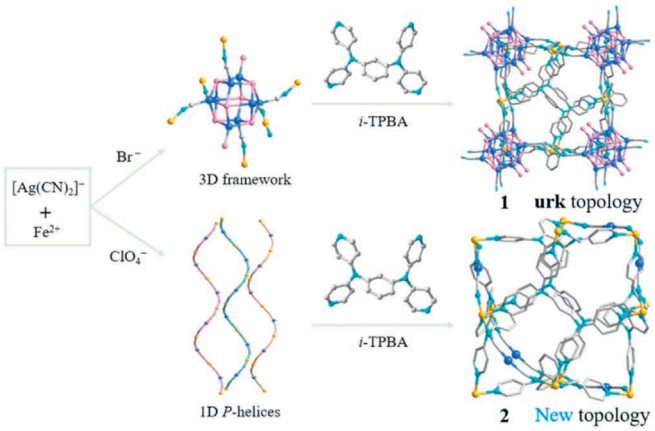



**Fig. 1.** Reaction scheme for the synthesis of **1** and **2**. Color codes: Fe, golden yellow; C, gray; Br, pink; Ag, blue; N, sky blue. Hydrogen atoms, solvent molecules and disordered components are omitted for clarity.

**T108** topology. Clearly, the self-assembly of these products is highly dependent on the nature of the anions.

Here, instead of TPBA, the isomeric tetrapyridyl ligand $N^1$,$N^1$,$N^3$,$N^3$-tetra(pyridin-4-yl)benzene-1,3-diamine (*i*-TPBA, Scheme 1) was employed to construct novel SCO MOFs. The reactions of *i*-TPBA and K[Ag(CN)$_2$] with FeBr$_2$ and Fe(ClO$_4$)$_2$·6H$_2$O in EtOH/DEF solution yielded distinct MOFs: [Fe$^{II}$$_3${Ag$_8$Br$_8$(CN)$_6$}(*i*-TPBA)$_3$]·4DEF (**1**, DEF = *N*,*N*-diethylformamide) featuring the **urk** topology and [Fe$^{II}${Ag(CN)$_2$}(*i*-TPBA)]ClO$_4$·2H$_2$O·0.5DEF (**2**) exhibiting a previously unreported topology. Furthermore, thiophene guest molecules were incorporated to form [Fe$^{II}$$_3${Ag$_8$Br$_8$(CN)$_6$}(*i*-TPBA)$_3$]·9thiophene (**1_thio**) and [Fe$^{II}${Ag(CN)$_2$}(*i*-TPBA)]ClO$_4$·4thiophene (**2_thio**), respectively. Consequently, the SCO behavior can be effectively modulated by the guest molecules, leading to a scan rate-dependent hysteretic SCO behavior observed in **2_thio**.

Yellow single crystals of **1** or **2** were obtained by the slow diffusion of K[Ag(CN)$_2$] and *i*-TPBA ligand into solutions of FeBr$_2$ or Fe(ClO$_4$)$_2$ in EtOH/DEF, respectively. This process resulted in the formation of crystals with distinct compositions and topologies. A thiophene solution was added to the mother liquor containing single crystals of **1** or **2** for 3 days, resulting in the deep yellow crystals of **1_thio** or **2_thio**, respectively. Although the crystal quality of **1_thio** was poor, its composition was confirmed *via* thermogravimetric analysis (Fig. S2 in Supporting information) and elemental analysis.

Single-crystal X-ray diffraction (SC-XRD) analysis reveals that **1** crystallizes in the trigonal $R\bar{3}c$ space group at 240 K (Tables S1 and S2 in Supporting information). The asymmetric unit contains only one-sixth of the chemical formula (Fig. S7 in Supporting information). The structure features a centrosymmetric cluster anion [Ag$_8$Br$_8$(CN)$_6$]$^{6-}$, which acts as a secondary building block (Fig. 1). Six Ag1 and two Ag2 ions form a distorted cube with weak argentophilic interactions, in which the Ag1···Ag1 and Ag1···Ag2 contacts are 3.276 and 3.702 Å (Table S2 in Supporting information), respectively. Each face of the Ag cube is covered by a $\mu_4$-Br1$^-$ ion, resulting in a nearly rhombic dodecahedral [Ag$_8$Br$_6$]$^{2+}$ cage. Each Ag1 ion is tetrahedrally coordinated by three $\mu_4$-Br1$^-$ ions and one C atom from the CN$^-$ ligand. The Ag2 ion is coordinated by three $\mu_4$-Br1$^-$ ions and one terminal Br2$^-$ ion. Two Ag2 and two Br2$^-$ ions are located on the 3-fold rotoinversion axis as well as the *c*-axis.

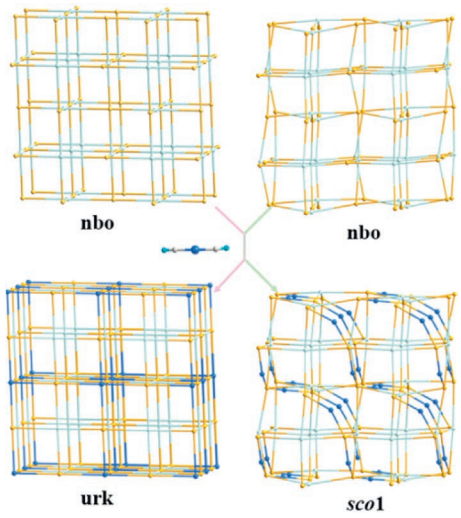



**Fig. 2.** The topological networks of the organic connectivity (up) and the overall framework (down) in **1** (left) and **2** (right). Color codes: Fe, golden yellow; *i*-TPBA, cyan; [Ag$_8$Br$_8$(CN)$_6$]$^{6-}$ cluster, blue; Ag(CN)$_2$$^-$, blue.

Each Fe$^{2+}$ ion is axially coordinated by two cyanide ligands from two [Ag$_8$Br$_8$(CN)$_6$]$^{6-}$ clusters. The [Ag$_8$Br$_8$(CN)$_6$]$^{6-}$ clusters serves as hexatopic nodes to axially connect six Fe$^{2+}$ ions, forming a 3D inorganic network with **pcu** topology (Fig. S11 in Supporting information). Each Fe$^{2+}$ ion is further equatorially coordinated by four tetradentate *i*-TPBA ligands, resulting in a [FeN$_6$] coordination environment. The average Fe−N bond length is 2.182 Å at 240 K, corresponding to the HS state. Since the benzene ring of *i*-TPBA ligand is disordered in two positions, the whole *i*-TPBA ligand has an inversion center in the crystal structure. The *i*-TPBA ligands act as tetratopic nodes to equatorially connect four Fe$^{2+}$ ions, resulting in a 3D organic connectivity with **nbo** topology. Consequently, the integration of the 3D **pcu** inorganic connectivity and the 3D **nbo** organic connectivity results in an $I^3O^3$ hybrid inorganic-organic framework characterized by the **urk** topology (Fig. 2 and Fig. S12 in Supporting information) [22–25]. The DEF guest molecules are highly disordered and were omitted from the structure using the solvent mask in OLEX2 [26].

Compound **2** crystalizes in the trigonal *R*32 space group at 100 K (Tables S3 and S4 in Supporting information). The asymmetric unit consists of two unique Fe(II) ions with half occupancy, one [Ag(CN)$_2$]$^-$ linker, one *i*-TPBA ligand, one DEF molecule with half occupancy, two ClO$_4$$^-$ anions with one-third occupancy and one ClO$_4$$^-$ anion with one-sixth occupancy (Fig. S13 in Supporting information). The remaining ClO$_4$$^-$ anions and solvent molecules exhibit high disorder and were excluded from the structural refinement using a solvent mask in OLEX2 [26]. Each Fe(II) ion is coordinated by four *i*-TPBA ligands in the equatorial plane and by two [Ag(CN)$_2$]$^-$ linkers in the apical positions, forming a distorted octahedral [FeN$_6$] coordination environment. The average Fe1−N bond length is 2.051 Å at 100 K, which is close to the LS state. In contrast, the average Fe2−N bond length is 2.164 Å, corresponding to the HS state. Notably, the [Ag(CN)$_2$]$^-$ units axially bridge the Fe1 and Fe2 ions to construct a 1D right-handed

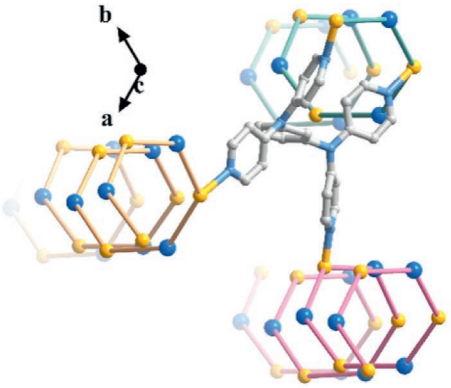



**Fig. 3.** View of the 1D helical chains interconnected *via* the *i*-TPBA ligands in **2**. Color codes: Fe, golden yellow; C, gray; N, sky blue; Ag, blue.

$3_1$ helical chain along the *c* axis (Fig. S14 in Supporting information), with the average bond angles of C−Ag−C = 168.47°, Ag−C≡N = 170.32°, C≡N−Fe = 163.39° and Fe1···Ag···Fe2 = 147.87°, respectively. This structure contrasts sharply with the 1D linear inorganic connectivity observed in the inverse-Hofmann-type MOF [Fe(TPB){Au(CN)$_2$}]I·4H$_2$O·4DMF (TPB = 1,2,4,5-tetra(pyridine-4-yl)benzene) (Fig. 3) [27]. The twisted tetradentate pyridyl ligand *i*-TPBA exhibits order in **2**, precluding the inversion center observed in **1**. Each *i*-TPBA ligand coordinates with four Fe(II) ions (Fe1, x, y, z; −y, x − y, z and Fe2, x, y, z; 1 − x + y, 1 − x, z) at the equatorial positions, generating a 3D M-Ligand-M connectivity with **nbo** topology (Fig. S15 in Supporting information). Consequently, each *i*-TPBA links three 1D right-handed helical chains, resulting in a 3D chiral framework (Fig. 3, Figs. S16 and S17 in Supporting information). The integration of the 1D chiral helical chain with the 3D **nbo** organic connectivity yields a $I^1O^3$ hybrid inorganic-organic framework. We define this unreported topology as ***sco*1**, which has been formally registered in the ToposPro program with the point symbol $\{3.5^3.6^2\}\{3^2.5^5.6^6.7^2\}$ (Fig. 2 and Fig. S20 in Supporting information) [28–31].

Compound **2_thio**, crystallizing in the *R*32 space group at 100 and 290 K, is obtained by soaking **2** in thiophene solution for 3 days (Tables S5 and S6 in Supporting information). The composition of the cationic framework in the asymmetric unit of **2_thio** at 100 and 290 K remains identical to that of **2** (Fig. S21 in Supporting information). At 100 K, three $ClO_4^-$ anions with one-third occupancy are resolved, exhibiting positional disorder around a $C_3$ rotation axis along the *c*-axis. Additionally, four thiophene guest molecules with the occupancies of 0.5, 1, 0.6 and 0.4 are identified at 100 K. This indicates that one and a half thiophene are too disordered to be solved. Only one thiophene molecule participates in the C-H···$\pi$ interaction with the *i*-TPBA ligand, reflecting a weak host-guest interaction (Fig. S22 in Supporting information). Upon increasing the temperature to 290 K, the $ClO_4^-$ anions and thiophene guest molecules exhibit high disorder and were excluded from the structural refinement using a solvent mask in OLEX2 [26]. The presence of thiophene is further confirmed by infrared (IR) spectroscopy and scanning electron microscopy (SEM) and energy dispersive spectrometer (EDS) (*vide infra*). The average Fe1−N bond lengths are 1.984 Å at 100 K and 2.190 Å at 290 K, corresponding to the LS and HS states, respectively, suggesting a spin transition process. The average Fe2−N bond lengths are 2.169 Å at 100 K and 2.207 Å at 290 K, consistent with the HS state. Meanwhile, the unit cell volumes of **2_thio** increase by 5.2 % during the SCO process.

The IR spectra were collected at room temperature to assist in identifying the molecular composition (Figs. S23−S26 in Supporting information). The presence of the counter anion $ClO_4^-$ is confirmed by its characteristic $\nu$(Cl−O) peaks, which appear at 1083 and 1090 cm$^{-1}$ for **2** and **2_thio**, respectively. Upon loading thiophene guest molecules, broad bands at 3080 and 3090 cm$^{-1}$ emerge in **1_thio** and **2_thio**, respectively, and can be attributed to the C-H stretching vibrations. Additionally, sharp peaks at 1432 and 1434 cm$^{-1}$ are observed in **1_thio** and **2_thio**, respectively, corresponding to the thiophene ring stretching vibrations.

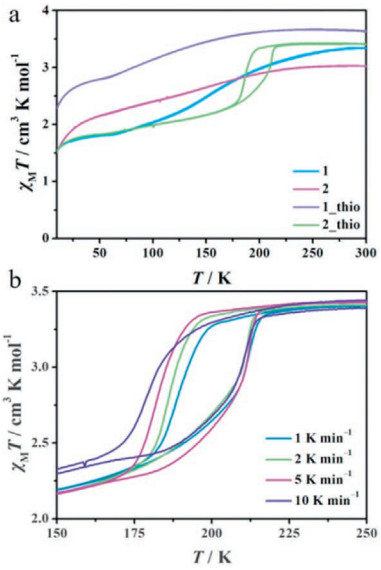



**Fig. 4.** (a) Magnetic data per Fe unit for **1**, **2**, **1_thio** and **2_thio** under a 0.5 T dc field. (b) Variable-temperature magnetic susceptibility data of **2_thio** at 1, 2, 5, and 10 K/min over the temperature range of 150–250 K.

The existence of the $ClO_4^-$ anion and thiophene guest molecule was further verified through SEM and EDS analyses (Figs. S27−S29 in Supporting information). Notably, the detection of the S element confirms the successful incorporation of thiophene guest molecules in **1_thio** and **2_thio**. Furthermore, the presence of the Cl element indicates the inclusion of the $ClO_4^-$ anion in **2_thio**.

Variable-temperature magnetic susceptibility data revealed the guest-dependent SCO behaviors (Fig. 4 and Figs. S30−S35 in Supporting information). For **1**, the $\chi_M T$ value per Fe(II) unit gradually decreases from 3.33 cm$^3$ K mol$^{-1}$ at 300 K to 1.54 cm$^3$ K mol$^{-1}$ at 10 K, indicating a gradual and incomplete SCO behavior. The subsequent warming curve overlaps with the cooling one, ruling out hysteretic SCO behavior. The first-order derivative of the magnetic data reveals a spin transition temperature ($T_{1/2}$) of 146 K. Upon incorporation of thiophene guest molecules, the $\chi_M T$ values of **1_thio** are consistently higher than those of **1**. The $\chi_M T$ value per Fe(II) unit slightly decreases from 3.64 cm$^3$ K mol$^{-1}$ at 300 K to 2.28 cm$^3$ K mol$^{-1}$ at 10 K. Consequently, **1_thio** exhibits a gradual and incomplete SCO behavior with a higher HS fraction compared to that of **1**.

For **2**, the $\chi_M T$ values per Fe(II) unit exhibit a decrease from 3.02 cm$^3$ K mol$^{-1}$ at 300 K to 1.51 cm$^3$ K mol$^{-1}$ at 10 K, reflecting to an incomplete and gradual SCO property. At 100 K, the $\chi_M T$ value based on the formula with one Fe(II) ion is measured as 2.41 cm$^3$ K mol$^{-1}$. This value is consistent with the near LS Fe1 and HS Fe2 ions, each with half occupancy, as revealed from the crystallographic data. The spin transition temperature for **2** is determined to be 147 K, which is comparable to that of **1**. However, the spin transition process in **2** is more gradual compared to that of **1**. This difference may be attributed to the higher octahedral distortion parameters $\Sigma$ (33.90° and 34.90°) observed in **2**, as opposed to 20.30° in **1**.

When the thiophene guest molecules are introduced in **2**, a hysteresis SCO behavior is observed with a sweep rate of 2 K/min in **2_thio**. As shown in Fig. 4a, the $\chi_M T$ value is 3.40 $cm^3$ K $mol^{-1}$ at 300 K, which is consistent with the HS Fe1 and Fe2 ions with half occupancy. It remains almost constant until 200 K, and quickly decreases to 2.34 $cm^3$ K $mol^{-1}$ at 175 K and then gradually decreases to 1.77 $cm^3$ K $mol^{-1}$ at 30 K. The crystallographic data reveal that the Fe1 ions switch from the HS to LS states while the Fe2 ion remain the HS state, which is consistent with the above incomplete SCO behavior. At lower temperature, the $\chi_M T$ value decreases slightly faster to 1.53 $cm^3$ K $mol^{-1}$ at 10 K, which may be attributed to the zero-field splitting and/or the weak antiferromagnetic interactions among HS Fe(II) ions. Upon heating, the magnetic curve moves to the high temperature region. The differential magnetic curves exhibit one peak at 186 and 211 K in the cooling and heating modes, respectively, illustrating a 25 K hysteresis loop. Obviously, the host-guest interactions contribute to the SCO cooperativity. The $\boldsymbol{\Sigma}$ values at 100 K in **2_thio** are 30.70° and 30.30° for Fe1 and Fe2 ions, respectively, which are smaller than those in **2**. They change to 35.46° and 29.75° at 290 K, indicating that the coordination environment can be influenced by the weak host-guest interactions.

Notably, the hysteretic SCO behavior of **2_thio** exhibits a dependence on the scan rate. Magnetic data were systematically collected at scan rates of 1, 2, 5 and 10 K/min (Fig. 4b). The magnetic curves in the cooling mode shift to the lower temperatures as the scan rates increases, indicating that the high-temperature phase is partially trapped upon rapid cooling. Conversely, the magnetic curves in the heating mode exhibit only minor changes. Consequently, the width of hysteresis loop increases from 23 K to 31 K as the scan rates rises from 1 K/min to 10 K/min. Four distinct types of scan rate dependence for thermal hysteresis have been reported in the literature: (1) Negligible scan rate dependence, (2) scan rate dependence observed exclusively in the cooling mode, (3) scan rate dependence observed exclusively in the heating mode, (4) scan rate dependence evident in both cooling and heating modes [32–34]. In this context, **2_thio** corresponds to type II. The HS molecule possesses a larger molecule size, unit cell volume and more distorted coordination environment compared to the LS molecule. Additionally, host-guest interactions in the high-temperature phase are weaker than those in the low-temperature phase, leading to reduced SCO cooperativity that fails to match the rapid decrease in temperature. Consequently, the HS state can be kinetically trapped at increasing rates during the cooling branch. Conversely, the nucleation of the larger HS molecules requires additional thermal energy to surmount the activation barrier in the heating mode and then rapidly grows to the thermodynamically favored HS state [35].

In summary, two distinct SCO MOFs were successfully self-assembled by reacting $FeBr_2$ and $Fe(ClO_4)_2{\cdot}6H_2O$ with $K[Ag(CN)_2]$ and the tetrapyridyl ligand *i*-TPBA. In **1**, the hexatopic $[Ag_8Br_8(CN)_6]^{6-}$ clusters, tetratopic organic ligands, and octahedral Fe(II) ion cooperatively assemble into a rare $I^3O^3$ hybrid inorganic-organic framework featuring **urk** topology. In contrast, the bent $[Ag(CN)_2]^-$ units in **2** axially coordinate to the Fe(II) ions, forming a 1D right-handed $3_1$ helical chain. The tetratopic *i*-TPBA ligands further interconnect three such helix chains, resulting in a homochiral $I^1O^3$ hybrid framework with a previously unreported topology designated as ***sco*1**. Both compounds **1** and **2** exhibit gradual and incomplete SCO behaviors. However, upon incorporation of thiophene guest molecules, **2_thio** displays a rare hysteretic and incomplete SCO behavior, where scan rate dependence is exclusively observed in the cooling mode. Notably, the width of the thermal hysteresis loop increases from 23 K to 31 K as the scan rates rises from 1 K/min to 10 K/min. This study demonstrates that SCO MOFs with novel topologies can be effectively self-assembled using multidentate ligands, providing a versatile platform for exploring multifunctional SCO materials.

## CRediT authorship contribution statement

**Guang Yang:** Writing – original draft, Methodology, Investigation, Formal analysis, Data curation, Conceptualization. **Lu Yu:** Writing – original draft, Methodology, Formal analysis, Data curation. **Ze-Yu Ruan:** Formal analysis, Data curation. **Ai-Qi Jian:** Formal analysis, Data curation. **Yan-Ru Chen:** Formal analysis, Data curation. **Yan-Cong Chen:** Formal analysis, Data curation. **Zhao-Ping Ni:** Writing – review & editing, Funding acquisition, Formal analysis, Conceptualization. **Ming-Liang Tong:** Writing – review & editing, Supervision, Funding acquisition, Conceptualization.

## Declaration of competing interest

The authors declare that they have no known competing financial interests or personal relationships that could have appeared to influence the work reported in this paper.

## Acknowledgments

This work was supported by the National Natural Science Foundation of China (NSFC, Nos. 22488101, 22271322), the Fundamental Research Funds for the Central Universities, Sun Yat-sen University (No. 24xkjc003), and the Graduate Student Scientific Research Innovation Project of Sun Yat-sen University (No. 02300–12240001).

## Supplementary materials

Supplementary material associated with this article can be found, in the online version, at doi:10.1016/j.cclet.2025.111656.

## References

[1] E. Resines-Urien, E. Fernandez-Bartolome, A. Martinez-Martinez, et al., Chem. Soc. Rev. 52 (2023) 705–727.
[2] M.K. Javed, A. Sulaiman, M. Yamashita, et al., Coord. Chem. Rev. 467 (2022) 214625.
[3] K.S. Kumar, M. Ruben, Angew. Chem. Int. Ed. 60 (2021) 7502–7521.
[4] E. Coronado, Nat. Rev. Mater. 5 (2020) 87–104.
[5] B. Weber, Coord. Chem. Rev. 253 (2009) 2432–2449.
[6] M.A. Halcrow, Chem. Soc. Rev. 40 (2011) 4119–4142.
[7] O. Kahn, C.J. Martinez, Science 279 (1998) 44–48.
[8] J.A. Real, E. Andrés, M.C. Munoz, et al., Science 268 (1995) 265–267.
[9] G.J. Halder, C.J. Kepert, B. Moubaraki, et al., Science 298 (2002) 1762–1765.
[10] Z.P. Ni, J.L. Liu, M.N. Hoque, et al., Coord. Chem. Rev. 335 (2017) 28–43.
[11] N. Sun, S.S.A. Shah, Z. Lin, et al., Chem. Rev. 125 (2025) 2703–2792.
[12] I.E. Khalil, J. Fonseca, M.R. Reithofer, et al., Coord. Chem. Rev. 481 (2023) 215043.
[13] W. Zhou, Y. Tang, X. Zhang, et al., Coord. Chem. Rev. 477 (2023) 214949.
[14] X. Li, K. Chen, R. Guo, et al., Chem. Rev. 123 (2023) 10432–10467.
[15] G.Z. Huang, Y.S. Xia, F. Yang, et al., J. Am. Chem. Soc. 145 (2023) 26863–26870.
[16] E. Coronado, M. Giménez-Marqués, G.Mínguez Espallargas, et al., J. Am. Chem. Soc. 135 (2013) 15986–15989.
[17] L. Piñeiro-López, M. Seredyuk, M.C. Muñoz, et al., Eur. J. Inorg. Chem. 2020 (2020) 764–769.
[18] M. Meneses-Sánchez, L. Piñeiro-López, T. Delgado, et al., J. Mater. Chem. C 8 (2020) 1623–1633.
[19] J. Troyano, F. Zamora, S. Delgado, Chem. Soc. Rev. 50 (2021) 4606–4628.
[20] F. Saraci, V. Quezada-Novoa, P.R. Donnarumma, et al., Chem. Soc. Rev. 49 (2020) 7949–7977.
[21] G. Cai, P. Yan, L. Zhang, et al., Chem. Rev. 121 (2021) 12278–12326.
[22] G. Yang, S.G. Wu, Z.Y. Ruan, et al., Angew. Chem. Int. Ed. 62 (2023) e202312685.
[23] G. Yang, Z.Y. Ruan, Y.C. Chen, et al., Angew. Chem. Int. Ed. 64 (2025) e202414330.
[24] A.K. Cheetham, C.N.R. Rao, R.K. Feller, Chem. Comm. (2006) 4780–4795.
[25] M.F. Wu, T.T. Shen, S. He, et al., CrystEngComm 17 (2015) 7473–7476.
[26] O.V. Dolomanov, L.J. Bourhis, R.J. Gildea, et al., J. Appl. Crystallogr. 42 (2009) 339–341.

[27] S.G. Wu, L.F. Wang, Z.Y. Ruan, et al., J. Am. Chem. Soc. 144 (2022) 14888–14896.
[28] V.A. Blatov, A.P. Shevchenko, D.M. Proserpio, Cryst. Growth Des. 14 (2014) 3576–3586.
[29] E.V. Alexandrov, V.A. Blatov, A.V. Kochetkov, et al., CrystEngComm 13 (2011) 3947–3958.
[30] F. Aman, A.M. Asiri, W.A. Siddiqui, et al., CrystEngComm 16 (2014) 1963–1970.
[31] C. Bonneau, M. O'Keeffe, D.M. Proserpio, et al., Cryst. Growth Des. 18 (2018) 3411–3418.
[32] R. Kulmaczewski, J. Olguín, J.A. Kitchen, et al., J. Am. Chem. Soc. 136 (2014) 878–881.
[33] H.Y. Sun, Y.S. Meng, L. Zhao, et al., Angew. Chem. Int. Ed. 62 (2023) e202302815.
[34] Z.Y. Li, Y.Y. Wu, Y. Li, et al., CCS Chem. 5 (2023) 412–422.
[35] S. Brooker, Chem. Soc. Rev. 44 (2015) 2880–2892.